Available online at www.sciencedirect.com
SCIENCE DIRECT
ELSEVIER
Polymer 46 (2005) 2306–2319
polymer
www.elsevier.com/locate/polymer

Thermodynamic, morphological, mechanical and fracture properties of poly(methyl methacrylate)(PMMA) modified divinylester(DVE)/styrene(St) thermosets

W.F. Schroeder[a], M.L. Auad[b], M.A. Barcia Vico[a], J. Borrajo[a,*], M.I. Aranguren[a]

[a]*Institute of Materials Science and Technology (INTEMA), University of Mar del Plata-National Research Council (CONICET), Av. Juan B. Justo 4302, 7600 Mar del Plata, Argentina*
[b]*Department of Material Science, University of Southern California (USC), 3651 Watt Way, 90089-0241 Los Angeles, CA, USA*

Received 12 June 2004; received in revised form 24 November 2004; accepted 12 January 2005

Abstract

Modified St/DVE cured materials were formulated with a commercial DVE_C ($M_n = 1015$ g/mol) and a synthesized (583 g/mol) DVE_L resins and styrene, adding a high molecular weight PMMA as modifier. A thermodynamic analysis of the initial miscibility for the St–PMMA and DVE–PMMA quasibinary systems was realized using the experimental cloud-point curves (CPC), in order to determine the binary interaction parameters. Calculated CPC for the quasiternary St/DVE/PMMA at 25 °C showed that St/DVE_L/PMMA is miscible in the whole concentration range, while the St/DVE_C/PMMA becomes partially miscible almost at the start of curing reaction (very low conversions). This miscibility behavior originates quite different morphologies in the systems cured at room temperature. Final materials with DVE_L showed typical nodular microphase morphologies generated by polymerization induced phase separation (PIPS) mechanism. Materials with DVE_C showed typical macrophase morphologies characterized by droplets-like domains, with secondary phase separation inside the droplets and in the mother phase. These morphological structures were directly related to the thermal and mechanical properties of the final systems. The low molecular weight resin generates a thermoset of higher glass transition temperature, bending modulus, and compression yield stress, but lower fracture resistance than the high molecular weight commercial resin. The addition of a thermoplastic modifier allowed to improve the fracture resistance without the unwanted reduction in modulus, which is inevitable when using elastomeric additives. The reason for the existence of an optimum modifier concentration is also discussed.

Keywords: Divinylester; Thermoplastic modifier; Cloud-point curves

1. Introduction

There is a great scientific and technological interest in the study and understanding of the structure and properties of modified styrene crosslinked divinylester resins (DVE), as well as unsaturated polyester resins (UP), because they are widely used as matrices in composites [1], sharing advantages, such as low room temperature viscosity coupled with rapid curing rate and low cost, plus the added chemical resistance in the case of DVE.

However, as it occurs with many thermoset polymers, the use of this type of resins is limited by their brittleness and the large shrinkage that occurs during polymerization. Although the addition of fillers and reinforcements could reduce the volume shrinkage, problems such as surface distortion, or development of internal cracks and voids could not be totally excluded [2]. Consequently, these resins are often used with modifiers to alleviate this problem, improving surface properties and/or toughness [3]. Many different low profile additives (LPA) have been investigated with the purpose of compensating volume contraction of the resin with a minimum cost for the other properties. Some of the more common LPA are polyethylene (PE), polystyrene (PS), poly(vinyl acetate) (PVAc), poly(methyl

* Corresponding author. Tel.: +54 223 481 66 00; fax: +54 223 481 00 46.
E-mail address: jborrajo@fi.mdp.edu.ar (J. Borrajo).

0032-3861/$ - see front matter © 2005 Elsevier Ltd. All rights reserved.
doi:10.1016/j.polymer.2005.01.019

methacrylate) (PMMA), poly(styrene-*co*-butadiene), and polyurethanes. Among them, PVAc and PMMA are the two low profile additives most widely used [4–7] and included in commercial formulations in the range of 5–20 wt% [5]. The use of thermoplastics offers two advantages over a more conventional elastomer modifier: it avoids the important loss of modulus that is a necessary consequence of adding rubber particles, and it absorbs significant amount of energy during fracture of the thermoset material, offering a toughening effect [8].

The morphology of the final modified networks, and the resulting mechanical properties depend on curing temperature, resin molecular weight and molecular weight distribution, additive concentration and its compatibility with the resin [5,9,10].

In this work, we are presenting a study on the effect of the addition of PMMA (initially solubilized in styrene, St) to a St–DVE network. The thermodynamic of the initial quasiternary system is discussed, and the final morphologies are presented and analyzed at the light of the thermodynamics of phase separation. Finally, the thermal and mechanical properties of the modified materials are reported and related to the observed microstructures.

2. Theoretical background

For a binary solution of polydisperse polymers, a general lattice theory expression for the dimensionless mixing Gibbs free energy, per mole of lattice sites, can be written as [11]:

$$\frac{\Delta G^{\mathrm{mix}}}{MRT} = \sum_{i=1}^{N_1} \frac{\phi_i}{r_i} \ln \phi_i + \sum_{j=1}^{N_2} \frac{\phi_j}{r_j} \ln \phi_j + g(T,\phi_2)\phi_1\phi_2 \qquad (1)$$

where, N_1 and N_2 are the total numbers of the components consisting of polymer 1 and polymer 2; ϕ_i and ϕ_j are the volumetric fractions of the i (polymer 1) and j (polymer 2) molecular species; $g(T,\phi_2)$ is a generalized Flory–Huggins interaction parameter dependent on temperature and composition; M factor is given by $M = \sum_{i=1}^{N_1} n_i r_i + \sum_{j=1}^{N_2} n_j r_j$ and represents the moles number of lattice sites in the system; n_i and n_j are the numbers of moles of the i and j molecular species; r_i, r_j are the relative molar sizes, defined by $r_i = V_i/V_r$ and $r_j = V_j/V_r$; V_i and V_j are the molar volumes of the i, j molecular species; V_r is the reference volume, usually taken as the molar volume of the smaller component or the smaller polymer monomeric unit.

In this work, $V_r = 116.85\ \mathrm{cm}^3/\mathrm{mol}$ was used, which corresponds to the molar volume of the styrene monomer.

In the usual applications of the simplest Flory–Huggins equation (F–H), the interaction parameter is considered to be a single function of the temperature, $\chi_{\mathrm{FH}} = d_0 + d_1/T$. However, it has been shown that the interaction parameter may also depend on both temperature and concentration [12]. Qian et al. [13] suggested a semiempirical form for $\chi(T,\phi_2)$ that allows the calculation of $g(T,\phi_2)$ in Eq. (1) as follows,

$$\chi(T,\phi_2) = g(T,\phi_2) - \phi_1 g'(T,\phi_2) \qquad (2)$$

where, $g'(T,\phi_2) = (\partial g(T,\phi_2)/\partial\phi_2)_T$. Upon integration of Eq. (2) at constant temperature, the relation between $\chi(T,\phi_2)$ and $g(T,\phi_2)$ is obtained,

$$\int_{\phi_2}^{1} \chi(T,\phi)\mathrm{d}\phi = \int_{\phi_2}^{1} (g(T,\phi) - \phi_1 g'(T,\phi))\mathrm{d}\phi$$
$$= (1-\phi_2) g(T,\phi_2) \qquad (3)$$

This last expression is introduced in Eq. (1) to obtain:

$$\frac{\Delta G^{\mathrm{mix}}}{MRT} = \sum_{i=1}^{N_1} \frac{\phi_i}{r_i} \ln \phi_i + \sum_{j=1}^{N_2} \frac{\phi_j}{r_j} \ln \phi_j + \phi_2 \int_{\phi_2}^{1} \chi(T,\phi)\mathrm{d}\phi \qquad (4)$$

The chemical potential $\Delta\mu_i$ for the species i of polymer 1 in the system is defined by

$$\Delta\mu_i = \left(\frac{\partial \Delta G^{\mathrm{mix}}}{\partial n_i}\right)_{P,T,n_{i\neq j}} \qquad (5)$$

and a similar relation holds for $\Delta\mu_j$ (specie j of polymer 2). The chemical potentials of species i and j can be derived from Eqs. (4) and (5); they are:

$$\frac{\Delta\mu_i}{RT} = 1 + \ln\phi_i - r_i\left(\frac{\phi_1}{r_{n1}} + \frac{\phi_2}{r_{n2}}\right) + r_i\chi(T,\phi_2)\phi_2^2 \quad (i = 1,\ldots,N_1) \qquad (6)$$

$$\frac{\Delta\mu_j}{RT} = 1 + \ln\phi_j - r_j\left(\frac{\phi_1}{r_{n1}} + \frac{\phi_2}{r_{n2}}\right) + r_j\chi(T,\phi_2)\phi_1\phi_2 + r_j\int_{\phi_2}^{1}\chi(T,\phi)\mathrm{d}\phi \quad (j = 1,\ldots,N_2) \qquad (7)$$

As it has been previously proposed by other authors [14,15], $\chi(T,\phi_2)$ is expressed as the product of two simple functions, one which is a unique function of the temperature, $D(T) = d_0 + d_1/T$, and the other a unique function of the concentration, $B(\phi_2) = (1 - b\phi_2)^{-1}$, where d_0, d_1 and b are constants for a given binary system. If the term $b = 0$, the simplest $\chi_{\mathrm{FH}} = D(T)$ is obtained.

Under constant temperature and pressure, a thermodynamic analysis of the liquid–liquid equilibrium in a quasibinary mixture of two polydisperse polymers, at the cloud-point conditions are given by the following equations:

$$\Delta\mu_i^{\alpha} = \Delta\mu_i^{\beta} \quad (i = 1,\ldots,N_1) \qquad (8)$$

$$\Delta\mu_j^{\alpha} = \Delta\mu_j^{\beta} \quad (j = 1,\ldots,N_2)$$

where α and β represent the mother and emergent phases in equilibrium.

In addition, an equation for the mass balance for the emergent β phase must be included in the analysis. This balance is given by

$$\sum_{i=1}^{N_1} \phi_1^{\alpha} W_i \exp(r_i \sigma_1) + \sum_{j=1}^{N_2} \phi_2^{\alpha} W_j \exp(r_j \sigma_2) = 1 \tag{9}$$

where W_i and W_j are the molecular species distributions of the polymers 1 and 2, respectively.

The solution of the equilibrium set of Eq. (8) and the mass balance, Eq. (9), must be solved simultaneously to obtain the cloud-point and shadow curves. The spinodal curve is obtained from the thermodynamic stability limit of the homogeneous phase, $\left|\Delta G^{\mathrm{mix}''}\right|_{T,P} = 0$, whose expression for a quasibinary polymer system is,

$$\frac{1}{r_{w1}\phi_1} + \frac{1}{r_{w2}\phi_2} - D(T)[2B(\phi_2) + \phi_2 B'(\phi_2)] = 0 \tag{10}$$

The equations developed in the thermodynamic treatment for quasibinary systems can be generalized to a quasiternary system consisting of polydisperse polymer 1, polydisperse polymer 2 and monomeric solvent (0), where only the interaction parameter between 1 and 2 is considered to be dependent on both temperature and concentration. The expression derived from the lattice theory for the dimensionless mixing Gibbs free energy per mole of lattice sites is given by the following Eq. (11)

$$\begin{aligned}\frac{\Delta G^{\mathrm{mix}}}{MRT} = {} & \frac{\phi_0}{r_0}\ln\phi_0 + \sum_{i=1}^{N_1}\frac{\phi_i}{r_i}\ln\phi_i + \sum_{j=1}^{N_2}\frac{\phi_j}{r_j}\ln\phi_j \\ & + \chi_{01}\phi_0\phi_1 + \chi_{02}\phi_0\phi_2 + \phi_1\phi_2\frac{1}{(1-\phi_2)} \\ & \times \int_{\phi_2}^{1}\chi(T,\phi)\mathrm{d}\phi\end{aligned} \tag{11}$$

This equation is proposed assuming that the residual ternary contribution to the mixing free energy is given by the addition of the three binary residual contributions. This assumption is a good first approximation for the description of a ternary phase diagram.

The chemical potentials of solvent 0, polymer 1 (i-mer) and polymer 2 (j-mer), $\Delta\mu_0$, $\Delta\mu_i$, and $\Delta\mu_j$, are directly derived from Eq. (11). The results are:

$$\begin{aligned}\frac{\Delta\mu_0}{RT} = {} & 1 + \ln\phi_0 - r_0 F(\phi, r) \\ & + r_0\left[\chi_{01}\phi_1(1-\phi_0) + \chi_{02}\phi_2(1-\phi_0) + \frac{\chi(T,\phi_2)\phi_1\phi_2^2}{(1-\phi_2)}\right. \\ & \left. - \frac{\phi_1\phi_2^2}{(1-\phi_2)^2}\int_{\phi_2}^{1}\chi(T,\phi)\mathrm{d}\phi - \frac{\phi_1\phi_2}{(1-\phi_2)}\int_{\phi_2}^{1}\chi(T,\phi)\mathrm{d}\phi\right]\end{aligned} \tag{12}$$

$$\begin{aligned}\frac{\Delta\mu_i}{RT} = {} & 1 + \ln\phi_i - r_i F(\phi, r) \\ & + r_i\left[\frac{\phi_2(1-\phi_1)}{(1-\phi_2)}\int_{\phi_2}^{1}\chi(T,\phi)\mathrm{d}\phi + \frac{\chi(T,\phi_2)\phi_1\phi_2^2}{(1-\phi_2)}\right. \\ & - \frac{\phi_1\phi_2^2}{(1-\phi_2)^2}\int_{\phi_2}^{1}\chi(T,\phi)\mathrm{d}\phi + \chi_{01}\phi_0(1-\phi_1) \\ & \left. - \chi_{02}\phi_0\phi_2\right]\end{aligned} \tag{13}$$

$$\begin{aligned}\frac{\Delta\mu_j}{RT} = {} & 1 + \ln\phi_j - r_j F(\phi, r) \\ & + r_j\left[\frac{\phi_1\phi_2}{(1-\phi_2)}\int_{\phi_2}^{1}\chi(T,\phi)\mathrm{d}\phi - \chi(T,\phi_2)\phi_1\phi_2\right. \\ & \left. + \phi_1\int_{\phi_2}^{1}\chi(T,\phi)\mathrm{d}\phi + \chi_{02}\phi_0(1-\phi_2) - \chi_{01}\phi_0\phi_1\right]\end{aligned} \tag{14}$$

where, $F(\phi, r) = \left(\frac{\phi_0}{r_0} + \frac{\phi_1}{r_{n1}} + \frac{\phi_2}{r_{n2}}\right)$; $i = 1, \ldots, N_1$ and $j = 1, \ldots, N_2$.

The equilibrium between two liquid phases in this quasiternary system was calculated from equating the chemical potential of each component in both phases, as follows:

$$\Delta\mu_0^{\alpha} = \Delta\mu_0^{\beta} \tag{15}$$

$$\Delta\mu_i^{\alpha} = \Delta\mu_i^{\beta} \quad (i = 1, \ldots, N_1)$$

$$\Delta\mu_j^{\alpha} = \Delta\mu_j^{\beta} \quad (j = 1, \ldots, N_2)$$

The mass balance equation for the emergent β phase is,

$$\phi_0^{\beta} + \sum_{i=1}^{N_1}\phi_1^{\alpha} W_i \exp(r_i\sigma_1) + \sum_{j=1}^{N_2}\phi_2^{\alpha} W_j \exp(r_j\sigma_2) = 1 \tag{16}$$

The solution of the equilibrium set of Eq. (15) and the mass balance, Eq. (16), must be solved simultaneously to obtain the cloud-point and shadow curves for the quasiternary mixture.

The spinodal curve (SC) for this quasiternary system is given by the following mathematical condition, which represents the stability limit of a homogeneous mixture $\Delta G_{11}''\Delta G_{22}'' - (\Delta G_{12}'')_{P,T}^2 = 0$, and its expression is:

$$\begin{aligned}& \left[\frac{1}{r_0\phi_0} + \frac{1}{r_{w1}\phi_1} - 2\chi_{01}\right]\left[\frac{1}{r_0\phi_0} + \frac{1}{r_{w2}\phi_2} - 2\chi_{02}\right. \\ & \left. + 2g'(T,\phi_2)\phi_1 + g''(T,\phi_2)\phi_1\phi_2\right] \\ & - \left[\frac{1}{r_0\phi_0} - \chi_{01} - \chi_{02} + g(T,\phi_2) + g'(T,\phi_2)\phi_2\right]^2 = 0\end{aligned} \tag{17}$$

In all the previous equations, the parameters r_{nk} and r_{wk} are the number and weight averages of the relative molar sizes of all molecular species in the k polymer component distribution. In the framework of the Flory–Huggins lattice theory, the two averages are related to different properties of the phase diagram; r_{nk} to the CPC, and r_{wk} to the SC.

3. Experimental

3.1. Materials and sample preparation

Two divinylester resins (DVE) were selected for the study. A resin of low molecular weight (DVE_L) was synthesized in our laboratory by reacting an epoxy resin, diglicidyl ether of bis-phenol A (DGEBA MY 790, Ciba Geigy, equivalent weight 176.2 g/equiv.), with methacrylic acid (Norent Plast S.A., laboratory grade reagent) using triphenylphosphine as catalyst (Fluka A.G., analytical reagent). The final conversion reached was higher than 93%, and it was stabilized with 300 ppm of hydroquinone. The second divinylester resin was a commercial resin, DVE_C, (PALATAL A 430, BASF AG). The molecular weights of both DVE were measured by size exclusion chromatography (Waters Model 510) with columns PLGel of 100, 500, 10^3, 10^4 and 10^6 Å (commonly used for oligomer characterization) and a refraction index detector (Waters 410) using polystyrene calibration. Its densities were experimentally measured using a precision balance (Becker and Sons).

The molecular parameter values for all the components used in this study are reported in Table 1.

Crosslinking reaction of the resins with or without modifier were realized by addition of styrene (St) in a weight proportion of St:DVE = 45:55, an usual commercial formulation. The cure reaction was carried out at room temperature for 24 h, followed by a postcuring at 170 °C for 1 h. The reaction was initiated by an amine-accelerated system using benzoyl peroxide 2 wt% (Luzidol 75%, Akzo Chemicals S.A.) as initiator and *N*,*N*-dimethylaniline 0.4 wt% (Akzo Chemicals S.A.) as promoter. All the materials were used as received.

The PMMA(239k) modifier utilized in this study was supplied by Subiton Laboratories, Buenos Aires, Argentina. For the thermodynamic analysis another PMMA(41k) was required (Aldrich Chemical Company). The molecular weights and the molecular species distributions of both PMMA were measured by SEC (Waters ALC 244, with columns Shodex A 802, 803, 804, 805 and 806/S) with refraction index and specific viscosity detection on line (Viscotek Model 200); using universal calibration.

The modified samples were prepared by addition of PMMA(239k) in a proportion of 5, 10 or 20% with respect to the total weight. The PMMA particles were initially dissolved in styrene and then, they were incorporated into the resin already mixed with the remaining styrene required to reach the St–DVE selected ratio.

Plates for bending tests (3 mm thickness) and fracture measurements (6 mm thickness) were obtained by casting the mixtures into moulds consisting of two glass plates coated with a silicone release agent, spaced by a rubber cord of the appropriate thickness and held together with clamps.

In order to make samples for compression testing, the reactive mixture of monomers (with or without additives) was injected into glass cylinders of 6 mm diameter previously sprayed with a silicone release agent. Compression specimens were carefully machined from the cylinders up to achieve the final dimensions (length/diameter = 1.5–2) with parallel upper and lower bases.

3.2. Cloud point curve determination

A series of binary mixtures with different compositions were prepared and introduced in a cell and subjected to controlled temperature programs. The cell was a glass cylinder-with-jacket of 10 cm^3 capacity. The fluid circulating in the jacket was supplied from an external bath at programmable heating rates. A rate of 2 °C/min was used in the heating and cooling programs. Cloud point temperatures of each binary solution were determined by visual observation and averaging the measured values of the onset of turbidity during cooling and the onset of transparency during heating. Each measurement was repeated at least five times to account for reproducibility. The solutions were thoroughly stirred during measurements to assure that the temperature was uniform throughout the sample.

Table 1
Physicochemical characteristics of the used components

	Styrene (St)(0)	DVE_L(1) synthesized	DVE_C(1) commercial	PMMA(2)(239k)	PMMA(2)(41k)
M_n (g/mol)	104	583[a]	1015[a]	239,000[a]	41,500[a]
M_w (g/mol)	–	618[a]	1766[a]	641,000[a]	80,000[a]
M_w/M_n	–	1.06	1.74	2.68	1.93
Density$_{25\ °C}$ (g/cm^3)	0.89[b]	1.16[b]	1.16[b]	1.12[c]	1.19[c]

[a] Measured by SEC, THF solvent at 1 ml/min.
[b] Measured using a precision balance for densities.
[c] Taken from the supplier's catalogue.

3.3. Electronic microscopy

Fractured specimens were gold coated and then observed by scanning electron microscopy (SEM), using a Jeol JSM 35 CF scanning microscope.

3.4. Physical and mechanical tests

Dynamic mechanical tests were performed using a Perkin–Elmer 7e on rectangular bars of 2 ± 0.1 mm thickness and 3 ± 0.1 mm width. A three point bending geometry was used with a span of 15 mm, at a frequency of 1 Hz and at a heating rate of 10 °C/min. The applied static stress was 0.5 MPa and the dynamic stress 0.35 MPa.

Flexural modulus and strength were measured using three point bending geometry, according to ASTM D 790-86 specifications, using an electromechanical INSTRON Universal Testing Machine model 4467.

Compression test specimens were deformed between metallic plates lubricated with molybdenum disulphide in a hydraulic INSTRON Universal Testing Machine Model 8501 according to ASTM D 695-85.

Fracture mechanics measurements were made at room temperature, using three-point bending geometry at a crosshead displacement rate of 10 mm/min using an INSTRON Universal Testing Machine model 4467. Test specimens were prepared by cutting rectangular bars from the slabs using a diamond saw. Central V-shaped notches were machined in the bars, then a razor blade was positioned in the notch and gently tapped to induce the growth of a natural crack ahead the blade. The stress intensity factor at the onset of crack growth, K_{IC}, was calculated following the ASTM D 5528-94 specifications, using single edge notched specimens (SEN).

4. Results and discussion

Usually, phase diagrams for quasibinary or quasiternary systems are presented using two sets of coordinates $T-\phi_2$ and $\phi_1-\phi_2$, respectively. They are different projections of the $T-P-\phi_i$ hypersurfaces representing different states of polymer fractionation during the liquid−liquid macrophase separation of these systems. As a consequence, the CPC and the shadow curve (ShC), that represent the onset of phase separation in the system, do not superimpose with any of the coexistence curves (CCs), that would represent the system at different degrees of macrophase separation.

Under constant temperature and pressure, thermodynamic requirements for liquid−liquid phase equilibrium, at the cloud-point or coexistence conditions, in a mixture with polydisperse components are given by the Eqs. (8) and (15) for quasibinary and quasiternary systems, respectively.

Numerical methods to analyze and calculate CPC, ShC, SC, and CCs, in mixtures with polydisperse components have been proposed and discussed in the literature [11,12, 16–18]. The procedure developed by Kamide et al. for quasibinary [19] and quasiternary [20] solutions was used in this study.

4.1. Quasibinary systems

4.1.1. St(0)–DVE(1)

St(0)–DVE_C(1) quasibinary mixture was analyzed by Auad et al. in a previous paper [21]. The CPC of the experimental results presents upper critical solution temperature (UCST) behavior, and the simplest F–H thermdynamic model was applied in the calculation, taking the polydispersity into account. The constants corresponding to the expression of the interaction parameter as a function of the temperature are given in Table 2.

4.1.2. St(0)–PMMA(2)

Fig. 1 shows the experimental cloud point diagram for the system formulated with St(0) and PMMA(239k)(2). An UCST behavior is observed in this system. The experimental CPC was analyzed with Eqs. (6)–(9) to obtain the interaction parameter χ_{02} at each temperature with the assumption of χ-parameter is only temperature dependent and not concentration or molecular weight dependent.

Schulz–Zimm (S–Z) distribution function was used to represent the distribution of PMMA(239k) molecular species. This distribution corresponds to that of the mother α phase, since at the cloud point condition, only an infinitesimal amount of PMMA is in the emergent phase. In order to simplify the calculation procedure, a discrete distribution including 40 pseudo-species was used in the model instead. The average molecular weights M_n and M_w calculated with the discrete distribution are in good agreement with those measured by SEC. In Table 3 the number and weight relative molar volume averages, obtained with the discrete distribution and SEC are compared. During the calculation, the PMMA(239k) molecular mass-fraction distribution, given by S–Z, was truncated at $r_i = 20{,}000$ (molecular weight $M_i = 2.6 \times 10^6$ g/mol), since truncation at higher values did not change the results.

Fig. 2 shows the calculated χ_{02} values plotted versus $1/T$. The best fitting parameters are given in Table 2. Inverse calculation of CPC, ShC and SC was performed using the expression found for the χ-parameter. The curves plotted in Fig. 1 represent the results of the calculations. As can be

Table 2
Constants d_0, d_1, and b, of the interaction parameter equation

Binary pair	d_0	d_1 (K)	b
St(0)–DVE_C(1)[a]	−0.330	325.1	–
St(0)–PMMA(239k)(2)	−1.028	443.4	–
DVE_C(1)–PMMA(41k)(2)	−0.252	93.7	−2.815

[a] Ref. [21].

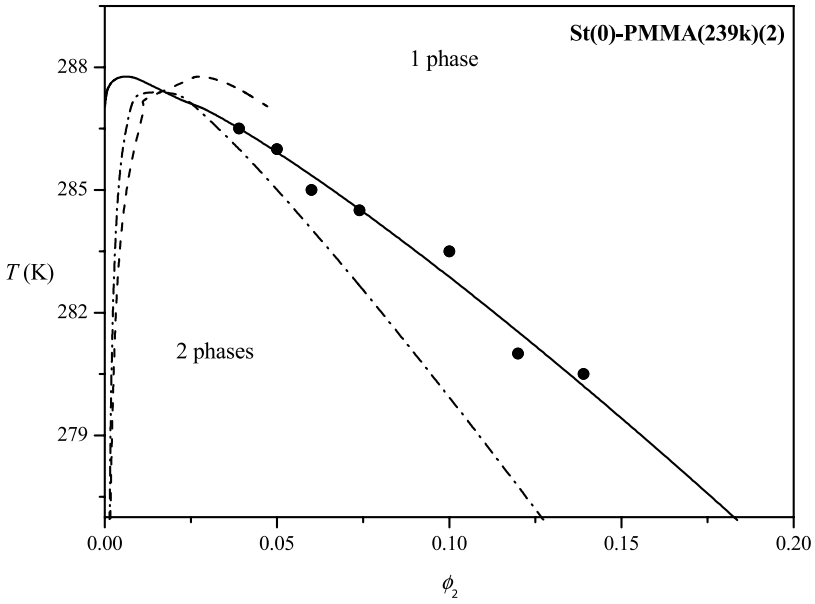

Fig. 1. St(0)–PMMA(239k)(2) quasibinary system: (●) experimental cloud-point data; (—) calculated cloud-point curve; (– – –) calculated shadow curve; (– · –) calculated spinodal curve.

seen, experimental and calculated CPCs show very good agreement.

4.1.3. DVE(1)–PMMA(2)

Cloud-points corresponding to the liquid–liquid phase separation in DVE_C–PMMA(239k) solutions could not be measured, because the high viscosity of the system made extremely difficult the expulsion of bubbles generated during stirring. Instead a PMMA(41k) of lower molecular weight was used under the assumption that the χ-parameter was molecular weight independent. Fig. 3 shows the experimental cloud-points for DVE_C–PMMA(41k) system. The cloud point phase diagram shows an UCST behavior.

The mass-fraction distribution of DVE_C was obtained from the size exclusion chromatogram (SEC), while for the PMMA(41k) the S–Z distribution function was used. In both cases, in order to simplify the calculation procedure, discrete distributions including 40 pseudo-species were used without a significant effect on the original distributions. In Table 3, the number and weight averages of the relative molar volumes obtained with the discrete and SEC distributions are compared.

When the experimental CPC was analyzed with Eqs. (6)–(9) to obtain the composition independent interaction parameter χ_{12}, it was found that it increases with temperature, as shown in Fig. 4. This calculated behavior is characteristic of phase diagrams with lower critical solution temperature (LCST), where χ_{12} increases when T increases, and it is contrary to the experimental evidences (the system is homogeneous at higher temperatures and is phase separated at lower temperatures). This failure of the simplest thermodynamic model is corrected considering that the interaction parameter for this quasibinary system is a function of T and ϕ_2, as it was proposed.

The results calculated with Eqs. (6)–(9), using the expression for the temperature and concentration dependent χ-parameter, lead to a temperature-dependent term, $D(T)$, whose behavior agree well with the experimental results exhibiting an UCST–CPC phase diagram [13,22,23]. Fig. 4 shows the temperature dependent factor $D(T)$ versus $1/T$, and the corresponding excellent linear fit. The calculated parameters for the temperature and composition terms are reported in Table 2.

The inverse calculation using the $\chi(T,\phi)$ values obtained from $D(T)$ and $B(\phi_2)$ functions, allow to obtain the CPC, ShC and SC curves, which are shown in Fig. 3. Comparing experimental and calculated CPCs, it can be concluded that

Table 3
Comparison between the number and weight relative molar volume averages obtained by SEC and pseudocomponents discrete distribution

	DVE_C		PMMA(239k)		PMMA(41k)	
	SEC	Discretized	SEC	Discretized	SEC	Discretized
r_n	8.14	8.15	1828	1840	317.0	317.3
r_w	14.16	14.11	4902	4862	612.2	612.2

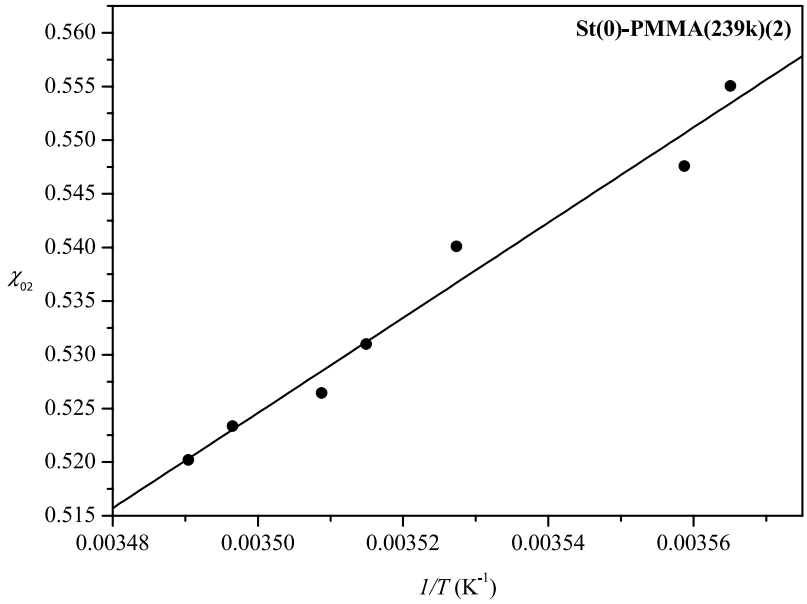

Fig. 2. Temperature dependence of the St(0)–PMMA(239k)(2) interaction parameter: (●) values calculated from the experimental cloud-point data; (—) results of the linear regression equation.

$\chi(T,\phi)$ describes very well the experimental quasibinary cloud-point phase diagram for this system.

4.2. St(0)–DVE(1)–PMMA(2) quasiternary system

In a general way, the CPC phase diagram of the St(0)–DVE(1)–PMMA(2) quasiternary physical mixture represents the initial state of the reactive system, when the reactive double bonds conversion equals zero, $P=0$. A good estimation of the CPC for this quasiternary system has been calculated by the combination of the required thermodynamic condition for the phases equilibrium, Eq. (15); the expression for the chemical potentials of the 0, 1i and 2j molecular species, Eqs. (12)–(14); and the mass balance equation for the β phase, Eq. (16). Calculated equilibrium compositions for the two liquid phases, at the cloud-point condition, allow determinate the CPC for the mother phase and the ShC for the emergent phase.

During calculation, it was assumed that the residual part of the mixing Gibbs free energy for the ternary system, Eq. (11), is constituted by the addition of the previously calculated binary interaction parameters χ_{01}, χ_{02} and g_{12}.

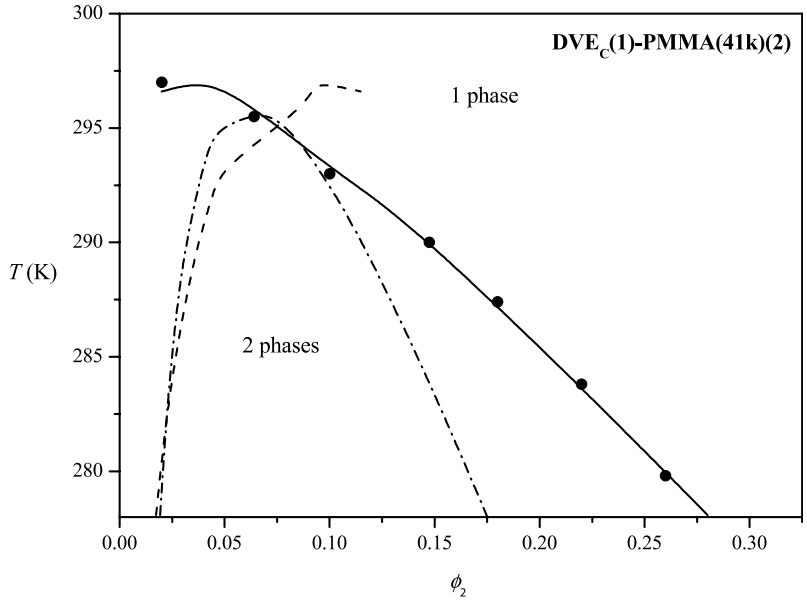

Fig. 3. DVE$_C$(1)–PMMA(41k)(2) quasibinary system: (●) experimental cloud-point data; (—) calculated cloud-point curve; (– – –) calculated shadow curve; (– · –) calculated spinodal curve.

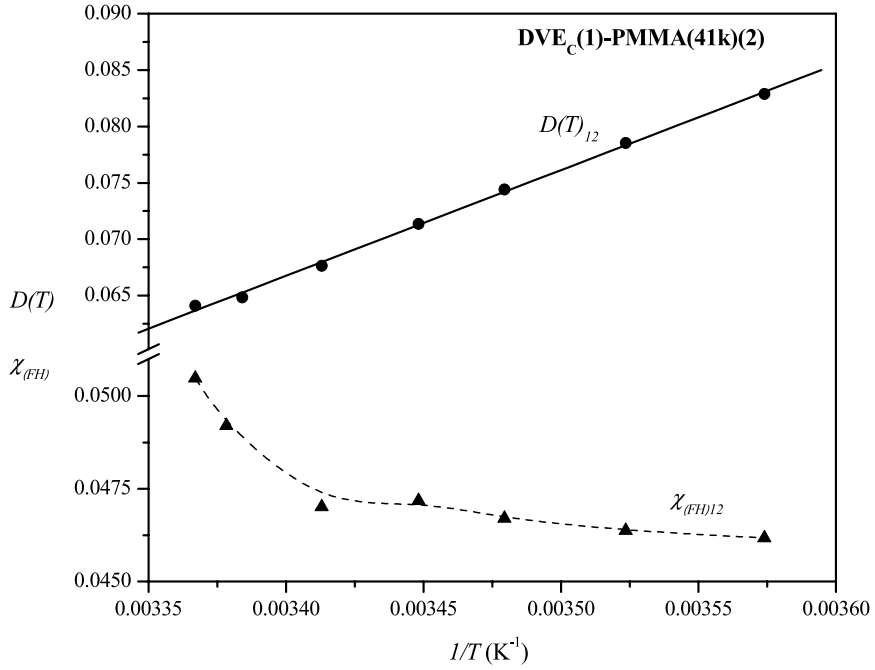

Fig. 4. Temperature-dependent term, $D(T)$, and F–H interaction parameter, $\chi_{(FH)}$, versus $1/T$ for the DVE_C(1)–PMMA(41k)(2) quasibinary system: (▲) and (– – –) are the $\chi_{(FH)}$ values calculated from the experimental cloud-point data and the fitted curve; (●) and (—) are the $D(T)$ values calculated from the experimental cloud-point data and the results of the linear regression equation.

At a given temperature, the resulting three equations system (12)–(16) can be solved numerically for the unknown independent global compositions, (ϕ_1^{α}, ϕ_2^{α}) and (ϕ_1^{β}, ϕ_2^{β}), assuming one them as fixed. In this way, the CPC and ShC can be predicted. In the calculations, each polydisperse component was represented by the same distribution function that was used in the analysis of the corresponding quasibinary. In this quasiternary system, the higher molecular weight PMMA(239k) was used in the essays and analysis.

Fig. 5 shows calculated CPC, ShC and SC for the St–DVE_C–PMMA(239k) quasiternary system at 25 °C. The points in this figure show the global compositions of the prepared materials, 0, 5, 10, and 20 wt% PMMA(239k) in a

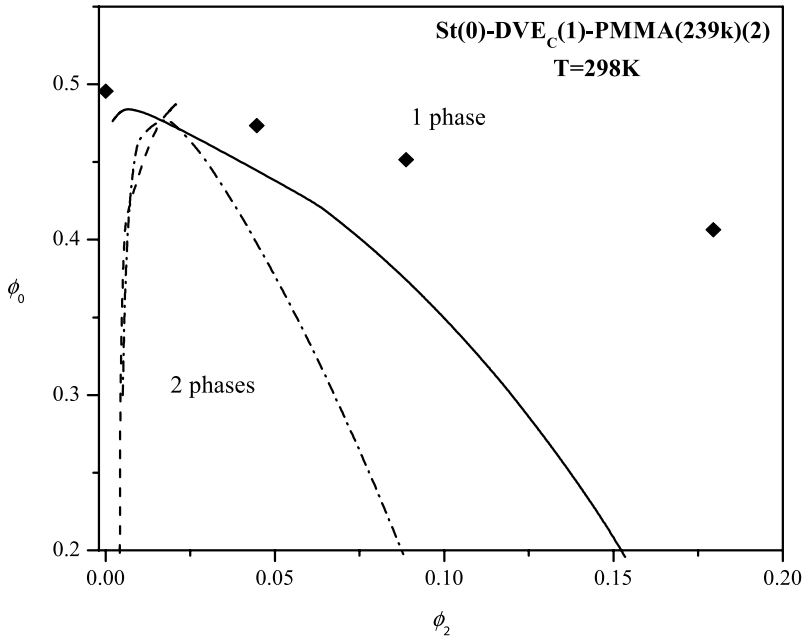

Fig. 5. St(0)–DVE_C(1)–PMMA(239k)(2) quasiternary system at 298K: (—) calculated cloud-point curve; (– – –) calculated shadow curve; (– · –) calculated spinodal curve; (◆) global compositions of prepared materials, 0, 5, 10 and 20 wt% PMMA(239k) on a constant weight proportion of DVE_C:St = 55:45.

liquid mixture of St:DVE = 45:55 (constant weight proportion). As it can be observed, these materials compositions are close to the estimated CPC phase diagram at $P = 0$ conversion. From this behavior it can be predicted that the quasiternary mixtures will be homogeneous, in all concentrations range, from room to higher temperatures.

4.3. Cured systems

The DVE–St system was copolymerized using benzoyl peroxide as initiator and *N*,*N*-dimethylaniline as promoter of the reaction. The resultant material is an amorphous thermoset, whose final properties are a function of the selected resin and modifier and initial composition of the system. In the study of the cured materials, only mixtures prepared in a weight proportion of 45:55 (St:DVE) and different concentrations of PMMA(239k) will be considered.

4.3.1. Morphology

The morphology of the final cured materials show marked differences depending on the molecular weight of the divinylester resin used in the formulation, and these differences show a correlation to the final properties of the materials, as it will be further discussed.

In the case of the low molecular weight resin, the mixture St–DVE_L–PMMA(239k) is initially homogeneous, because the high entropic contribution to the miscibility of the ternary system originated by the DVE low molecular weight component. Ternary CPC is not showed in Fig. 5 because at 25 °C this system is miscible at all compositions. Phase separation needs a significant progress in conversion in the pregel region of the crosslinking reaction, to widen the immiscibility area so that it superpose to the points representing the global compositions of the system (points in Fig. 5). As a consequence of the copolymerization reaction, phase separation takes place by the PIPS mechanism (polymerization induced phase separation). The formation of a St–DVE_L copolymer in the pregel state increases the viscosity and the incompatibility of this new component with the PMMA(239k) modifier until phase separation begins. Because the initial mixture was initially homogeneous, and the PIPS begins at conversions below the gel point (ca. 4–8%, [24]) the entire material suffers this process. This is clearly seen in Fig. 6(a), that the SEM micrograph for the St–DVE_L sample modified with 10% PMMA(239k). A larger magnification (Fig. 6(b)) allows to observe that the whole sample shows irregular nodules and that the fracture surface is quite irregular. Previous studies on St–DVE systems modified with elastomers [25,26] or with different thermoplastics [27,28] have shown that the nodules are formed by 'nanogels' of the St–DVE rich phase partially coalesced. These nodules are coated by the PMMA rich phase, which was segregated from the St–DVE_L rich phase during the curing reaction. It has been previously reported that this type of morphology generated in elastomer modified divinylester resins, leads to materials of low cohesion and reduced properties [29]. In the present case, due to the better properties of the thermoplastics at room temperature this problem is somehow alleviated.

The morphology developed in the higher molecular weight resin system (Fig. 7(a) and (b)) presents two regions well differentiated: a St–DVE_C copolymer rich phase and a PMMA(239k) rich phase. The latter is the discontinuous phase and presents a very complex internal microstructure, consisting in St–DVE_C nodules surrounded by PMMA modifier. The PMMA rich phase can show a very large distribution of sizes, from simple inclusions of a less than 1 μ to huge droplets close to 100 μ. Fig. 7(a) and (b) illustrates this feature for the St–DVE_C system modified with 10% (by wt) of PMMA(239k). This microstructure is the result of the initial miscibility at the beginning of the copolymerization reaction, and its evolution during curing. As shown in Fig. 5, the CPC of the St–DVE_C–PMMA(239k) quasiternary system is very close to the overall system compositions (points in this figure), and just a small increment in the conversion is needed for the start of the phase separation. Since, the system viscosity is low when the phase separation start, the emergent phase coalesces. In this way, the reactive system will be phase separated from almost the beginning of the curing reaction, forming two liquid phases. The droplets rich in PMMA that are formed in the pregel region, at the beginning of the reaction, correspond to the large domains observed in the micrographs. These domains are not initially neat PMMA but contain also some St and DVE_C, which react inside the droplet, forming microgels and undergoing the PIPS mechanism described before. On the other hand, in the main phase (St–DVE_C rich phase), there is also some PMMA dissolved and so smaller droplets are formed at different reaction times, in which interior the PIPS mechanism takes place. There are also some simple PMMA inclusions, which can be seen as some of the smaller 'holes' in the main thermoset phase (Fig. 7(b)). Similar structures have been previously described for UP modified with PVAc [2,30] and with PMMA [31,32]. Features typical of brittle fracture, smooth planes and river marks are observed in the main phase.

4.3.2. Thermal characterization

This characterization was carried out using dynamic mechanical measurements. The information obtained from this technique is illustrative of the network structure and the mechanisms involved during its formation.

Figs. 8 and 9 show representative curves obtained for the two series of modified thermosets. The St–DVE_L system produces networks with higher glass transition temperature than the St–DVE_C system, measured as the temperature at the maximum in tan δ (160 and 132 °C, respectively). This difference is the result of the shorter chains of the divinylester resin DVE_L, which produces a tighter network through end groups-crosslinking. Due to this feature,

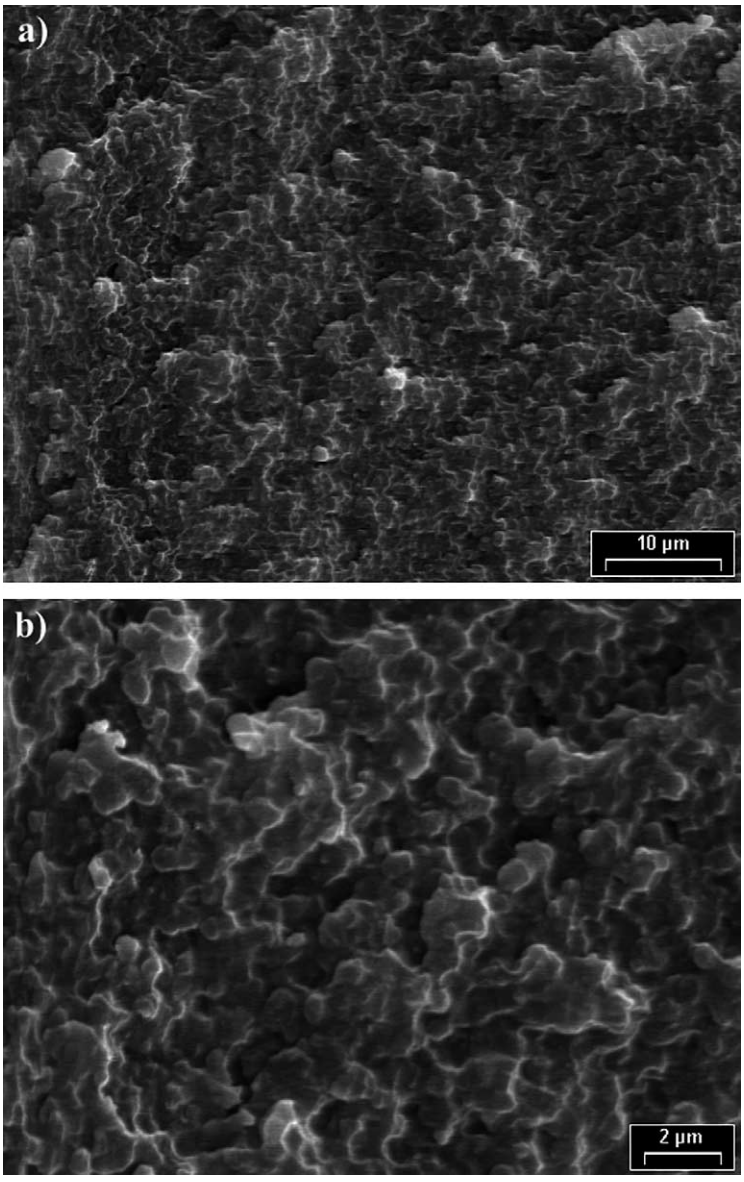

Fig. 6. SEM micrographs of the fracture surface for the DVE_L–St sample modified with 10% PMMA(239k) (a) at 2000×, and (b) at 6000×.

coordinated movements of a higher number of chains are needed in order to relax the material, higher energy is required for achieving chain mobility and so, the tan δ peak appears at higher temperatures for the system obtained from the low molecular weight resin. It is also interesting to notice that the height of tan δ peak is higher for St–DVE_C than for the St–DVE_L system (1.06 and 0.68, respectively), suggesting that more material is involved in the relaxation process.

Comparison of the glassy and the rubbery regions for the two series of networks shows higher values of the moduli for the St–DVE_L system, which is reasonable expected according to the crosslinking density of the networks. The differences are more clear in the rubbery region, where the moduli of the neat networks are 40 and 10 MPa for the low molecular weight and commercial resin-systems, respectively.

The addition of PMMA(239k) also modifies the dynamic mechanical response. In both cases, the drop of the modulus in the transition is shifted to lower temperatures, but it is interesting to notice that no major changes appear neither in the value of the glassy nor in the rubbery moduli in the St–DVE_C system. This would indicate that the crosslinking density of the network has not suffered much with the addition of the thermoplastic modifier. This is not the case for the St–DVE_L system, since the rubbery modulus decreases from 40 MPa to about 21 MPa with the addition of 20% PMMA(239k). This observation suggests that the crosslinking density has decreased with the PMMA addition, because less reactive groups have participated of

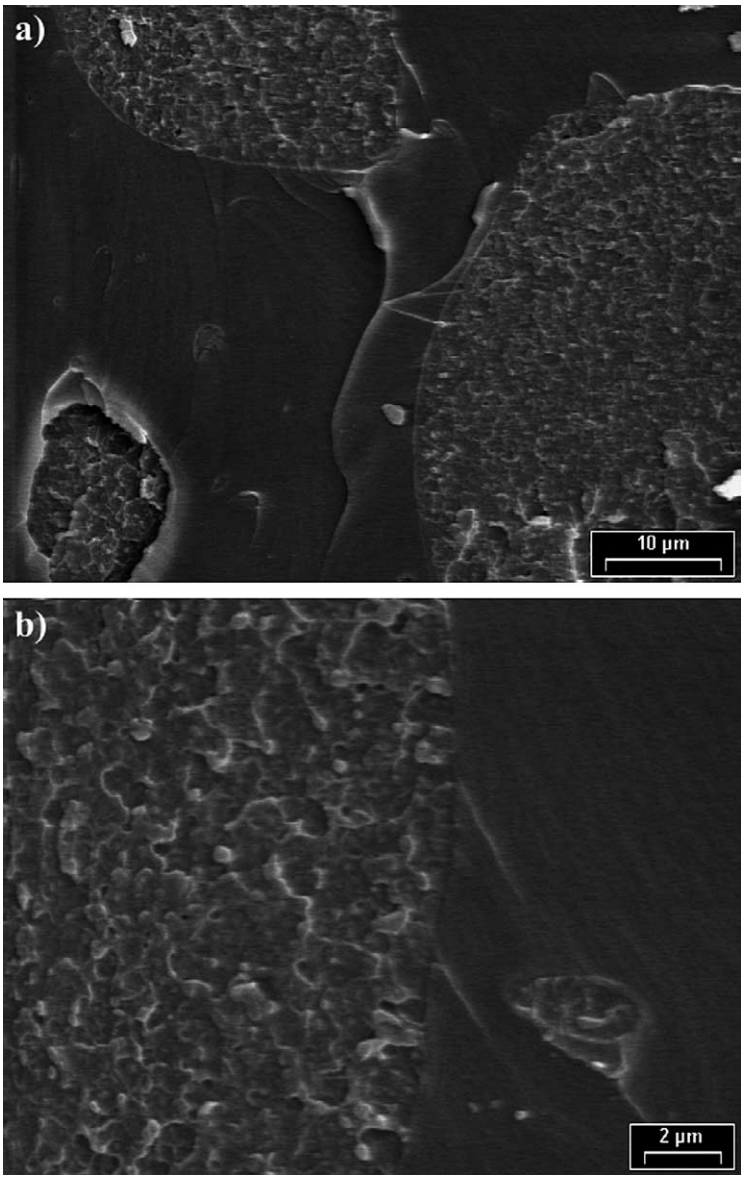

Fig. 7. SEM micrographs of the fracture surface for the DVE_C–St sample modified with 10% PMMA(239k) (a) at 2000×, and (b) at 6000×.

the reaction or because the thermoplastic is acting as a diluent in the crosslinked phase.

Further, inspection of the tan δ curves in Figs. 8 and 9 show clearly, that there are two transitions in the modified networks, corresponding to the two phases formed, the transition of the PMMA rich phase at the lower temperature and the transition of the St-resin rich phase at the higher temperature. There is also a difference between both systems: the two peaks appear more clearly separated in the commercial system. The glass transition temperature corresponding to the continuous phase (St–DVE_C rich phase) appears at the same temperature in all the series, the same is also true for the PMMA transition, which does not suffer any shift at different modifier concentrations. Varying the PMMA(239k) concentration from 5 to 10% produced only a slight increment in the height of the corresponding transition peak. The tan δ curves, as well as the observed invariance of the rubbery modulus of the series is indicating that the two phases are well separated and the immiscibility of the system appeared at the very beginning of the reaction. Thus, the density of crosslinking of the main phase did not vary with the modifier addition, even more the ratio St to DVE_C of the material trapped into the separated PMMA rich phase must be very similar to that of the main phase (again in agreement with an early phase separation occurring much before gelation). These observations are strongly supported by the SEM morphologies discussed in a previous section.

On the other hand, the tan δ peaks corresponding to the two transitions appear overlapped in the St–DVE_L system, which indicated that the two phases are not well separated. A closer observation of the curves, shows that there is a very slight shift in the transition peak of the St–DVE_L phase

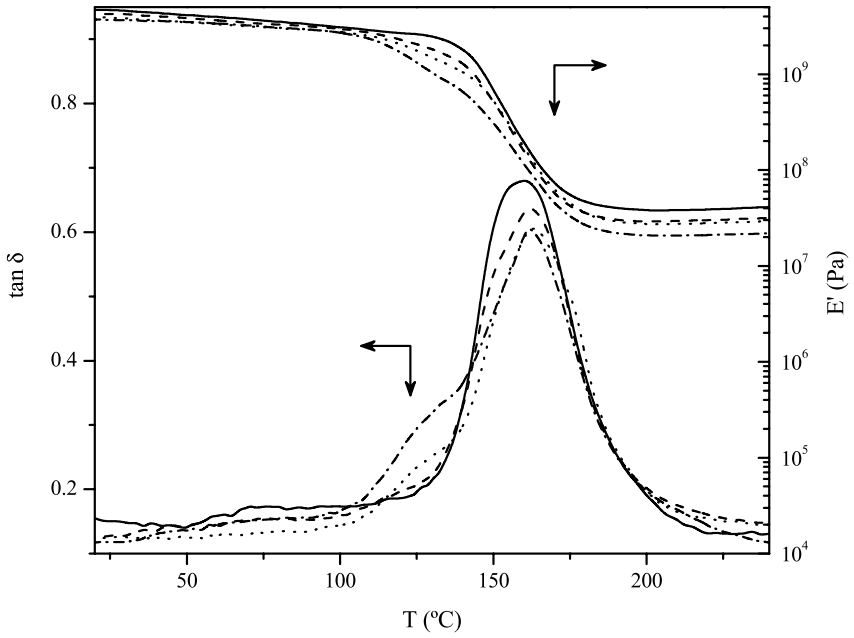

Fig. 8. Dynamic mechanical behavior as a function of temperature of neat and PMMA(239k)-modified St–DVE_L thermosets. Unmodified system (—). Modified mixtures with several amounts of PMMA: 5% wt (– – –), 10% wt (···), 20% wt (– · –).

towards higher temperatures (160–162 °C), as PMMA(239k) is added. This small difference can be explained by St-resin ratios that vary from the initial ratio, because of the partial miscibility of St in the PMMA phase. Because the separation phase takes place at higher conversions than in the commercial system, a small drift of the St-resin ratio occurs. This would also explain the drop in the value of the rubbery modulus, which is a function of the crosslinking density and drops significantly with PMMA(239k) addition. The transition of the PMMA rich phase appears as a shoulder at a temperature of approximately 122–124 °C. Although the concentrations are as high as those used in the commercial system, the height of the peak is much lower, because the phase is not so well separated as in the previous case. The separation in the St–DVE_L system corresponds to a PIPS mechanism, so that both phases are clearly less segregated and mobility is much more restricted than in the commercial system. Again, these

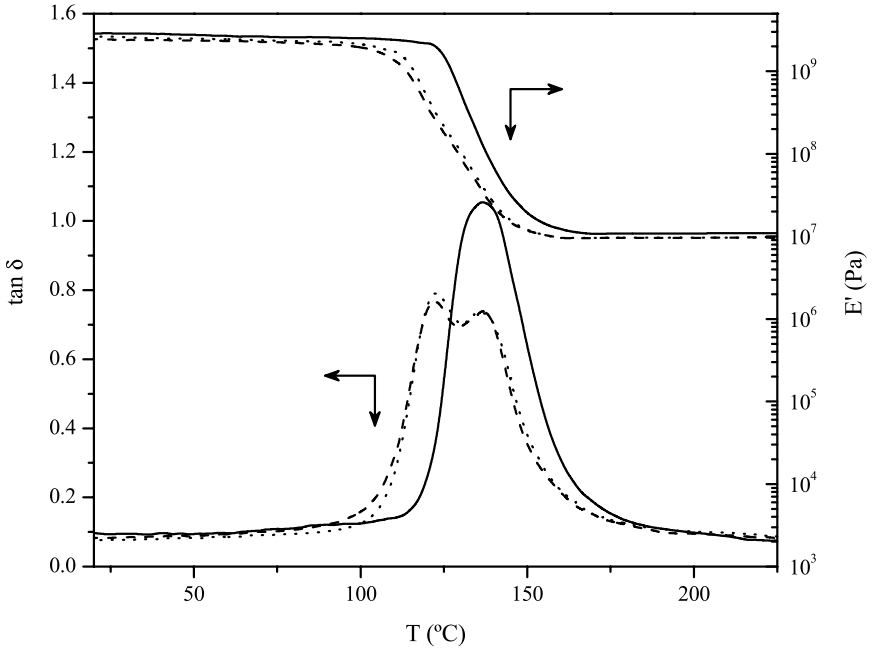

Fig. 9. Dynamic mechanical behavior as a function of temperature of neat and PMMA(239k)-modified St–DVE_C thermosets. Unmodified system (—). Modified mixtures with several amounts of PMMA: 5% wt (– – –), 10% wt (···).

Table 4
Mechanical properties of the networks prepared with the two different molecular weight DVE and varying concentrations of PMMA(239k) modifier

PMMA%	Flex. Mod., E_b (GPa)		Compres., σ_y (MPa)		K_{IC} (MPa $m^{1/2}$)	
	DVE_L–St	DVE_C–St	DVE_L–St	DVE_C–St	DVE_L–St	DVE_C–St
0	3.50±0.03	3.15±0.02	108.7±3.5	104.7±1.6	0.62±0.08	0.83±0.04
5	3.58±0.17	3.49±0.13	119.7±1.1	109.1±3.3	0.5±0.09	1.43±0.05
10	3.63±0.23	3.21±0.10	121.6±1.9	109.8±1.4	–	1.01±0.16

results are in perfect agreement with the phase separation phenomena described for each system and with the morphologies observed in Figs. 6 and 7 already discussed.

4.3.3. Mechanical characterization

Table 4 includes a summary of the mechanical (flexural and compression) and fracture behavior of the different materials obtained.

The system prepared with DVE_L shows higher flexural modulus, higher yield stress in compression and lower fracture resistance (lower K_{IC}) than the networks prepared from DVE_C commercial resin. This was to be expected from a low molecular weight resin that, as discussed before, leads to shorter chains between crosslinking points, and thus to a tighter network with less mobile chains.

As it was the aim of this study when choosing thermoplastic modifiers, the modulus of the materials were little affected by the addition of the modifiers. Actually, the mechanical properties were slightly improved, instead of the usual reduction observed when elastomers are added to the networks.

It is especially important to notice the improvement obtained in the fracture resistance of the St–DVE_C systems by addition of PMMA(239k). An optimum concentration is observed at 5 wt%, the same range observed in other systems by different authors [3,27,29,33]. Further addition produces a reduction of K_{IC}, because of the increment at the amount of droplets containing microvoids, which makes it easier for the cracks to advance. The low molecular weight resin does not show this improvement because microvoiding is generalized through the sample and crack finds an easy way to propagate through the voids plane.

5. Conclusions

Experimental CPC measurements for quasibinaries systems St–PMMA(239k) and DVE_C–PMMA(41k) were used to calculate the binary interaction parameters of these systems. The St–PMMA(239k) system can be described for a F–H parameter only temperature dependent. The DVE_C–PMMA(41k) system can not be analyzed with the simplest thermodynamic model and a temperature and composition dependent interaction parameter has been used. The thermodynamic analysis of the ternary phase diagrams allows us to say that the initial miscibility of the St–DVE_L–PMMA(239k) system is higher than that of the St–DVE_C–PMMA(239k). These differences are responsible for the quite different final morphologies of the cured samples at room temperature and are originated in the different DVE molecular sizes.

St–DVE_L–PMMA(239k) materials have a two phase micron size nodular morphology extended through the whole neat sample and originated by the PIPS mechanism. On the other hand, DVE_C formulated materials are macrophase separated in large drops of a PMMA(239k) rich phase with an internal nodular structure originated by the PIPS mechanism inside the drops. These drops are dispersed in a continuous phase rich in the reacted St–DVE_C copolymer.

The glass transition temperatures and the moduli values of these materials show a good correlation with the crosslinking density of the networks. The tan δ curves show clearly two transitions in the modified networks, corresponding to the PMMA rich and St–DVE rich phases formed. The two peaks appear more clearly separated in the commercial DVE systems indicating that the two phases are more segregated than in the DVE_L systems, which is in perfect agreement with the thermodynamic analysis predictions and the obtained material morphologies.

The final morphological structures were directly related to the thermal and mechanical properties of the cured materials. The low molecular weight resin generates a PMMA(239k) modified thermoset of higher glass transition temperature, bending modulus, and compression yield stress. The addition of PMMA(239k) produces toughening of the DVE_C networks, showing an optimum concentration at 5% wt This improvement was not obtained for the DVE_L system because of generalized microvoiding.

Acknowledgements

The financial support of Argentine institutions for promoting the science and technology CONICET, ANPCYT and the National University of Mar del Plata are greatly acknowledged.

References

[1] Abbate M, Martuscelli E, Musto P, Ragosta G, Scarinzi G. J Appl Polym Sci 1995;58:1825–37.
[2] Huang YJ, Su CC. J Appl Polym Sci 1995;55:305–22.
[3] Suspene L, Yang YS, Pascault JP. Additive effects on the toughening

of unsaturated polyester resins. In: Riew CK, Kinloch AJ, editors. Toughened plastics I: science and engineering, advances in chemistry series 233. Washington, DC: American Chemical Society; 1993. Chapter 7.
[4] Kinkelaar M, Muzumdar S, Lee LJ. Polym Eng Sci 1995;35:823–36.
[5] Cook WD, Zipper MD, Chung ACH. Polymer 1998;39(22):5431–9.
[6] Sun B, Yu TL. Macromol Chem Phys 1996;197:275–87.
[7] Gibson AG. Sheet moulding compounds. In: Jones FR, editor. Handbook of polymer–fiber composites. Essex: Longman Scientific and Technical; 1994. Chapters 3 and 3.17.
[8] Bucknall CB, Gilbert AH. Polymer 1989;30:213–7.
[9] Lucas JC, Borrajo J, Williams RJJ. Polymer 1993;34:1886–90.
[10] Oksman K, Clemons C. J Appl Polym Sci 1998;67:1503–13.
[11] Kamide K. In: Jenkins AD, editor. Thermodynamisc of polymer solutions: phase equilibria and critical phenomena, polymer science library 9. Amsterdam: Elsevier; 1990.
[12] Koningsveld R, Staverman AJ. J Polym Sci Part A-2 1968;6:305–23.
[13] Qian C, Mumby SJ, Eichinger BE. Macromolecules 1991;24: 1655–61.
[14] Bae YC, Shim JJ, Soane DS, Prausnitz JM. J Appl Polym Sci 1993;47: 1193–206.
[15] Choi JJ, Bac YC. Eur Polym J 1999;35:1703–11.
[16] Šolc K. Macromolecules 1970;3:665–73.
[17] Rätzsch MT. Makromol Chem Macromol Symp 1987;12:101–21.
[18] Mumby SJ, Sher P. Macromolecules 1994;27:689–94.
[19] Kamide K, Matsuda S, Shirataki H. Eur Polym J 1990;26:379–91.
[20] Shirataki H, Kamide K. Polym Int 1993;32:265–73.
[21] Auad ML, Aranguren MI, Borrajo J. Polymer 2001;42:6503–13.
[22] Siow KS, Delmas G, Patterson D. Macromolecules 1972;5:29–34.
[23] De Sousa HC, Rebelo LPN. J Polym Sci, Part B 2000;38:632–51.
[24] Matsumoto A, Okuno S, Aota H. Macromol Symp 1995;93:1–10.
[25] Auad ML, Proia M, Borrajo J, Aranguren MI. J Mater Sci 2002;37: 4117–26.
[26] Auad ML, Borrajo J, Aranguren MI. J Appl Polym Sci 2003;89(1): 274–83.
[27] Wang S, Wang J, Ji Q, Schultz AR, Ward TC, McGratz JE. J Polym Sci, Part B 2000;38:2409–21.
[28] Cao X, Lee LJ. J Appl Polym Sci 2003;90:1486–96.
[29] Auad ML, Frontini PM, Borrajo J, Aranguren MI. Polymer 2001;42: 3723–30.
[30] Muzumdar SV, Lee LJ. Polym Eng Sci 1991;31:1647–56.
[31] Don JP, Huang JG, Lee FH, Roan JW, Huang YJ. J Appl Polym Sci 2004;91:3369–87.
[32] Huang YJ, Liang CM. Polymer 1996;37:401–12.
[33] Huang YJ, Horng JC. Polymer 1998;39:3683–95.